On the electrical conductivity of composites with a polymeric matrix and a non-uniform concentration of carbon nanotubes

M.A.S. Matos, V.L. Tagarielli[1] and S.T. Pinho

Department of Aeronautics, Imperial College London, SW7 2AZ London, UK

Abstract

We present a multiscale modelling approach to explore the effects of a non-uniform concentration of carbon nanotubes (CNTs) on the electrical conductivity of CNT-polymer composites. Realistic three-dimensional representative volume elements (RVEs) are generated from a two-dimensional CNT concentration map, obtained via microscopy techniques. The RVEs capture the measured probability density function of the CNT concentration and include a length-scale to represent the details of the spatial distribution of the concentration. The homogenised conductivity of the RVEs is computed via multiscale FE analyses for different values of such length-scale, and it is compared to measurements. The modelling strategy is then used to explore the effects of the microstructural features of these materials on their electrical conductivity.

Keywords: (A) Carbon Nanotubes, (B) Electrical properties, (C) Multiscale modelling, Dispersion

Submitted to *Composites Science and Technology*, July 2019

* Corresponding author. E-mail v.tagarielli@imperial.ac.uk

1. Introduction

Enabling conductivity in engineering polymers allows a variety of technical applications, ranging from deformation and temperature sensors to electrostatic discharge and electromagnetic shielding [1, 2]. This can be achieved employing CNTs as a filler material, which also confer good mechanical, thermal and electrical properties at low weight. Due to the high aspect ratio of carbon nanotubes, very low CNT concentrations can form conductive networks in polymeric matrices [3, 4].

The processing conditions of CNT-polymer composites deeply influence the material microstructure, in turn resulting in significant effects on the electrical conductivity and the percolation thresholds, as summarized in [5]. The variation in the percolation thresholds reported by different authors is often attributed to a non-uniform CNT dispersion due to the surface features of the CNTs [6]: their high specific surface area and waviness favour van der Waals attraction, inducing agglomeration [7].

Several methods have been proposed to quantify the dispersion of CNT-polymer composites samples; most aim to measure parameters quantifying the free spacing between agglomerates, their size, and uniformity [8-11], and exploring correlations between these parameters and physical properties. Detailed low-scale observations, based on transmission or scanning electron microscopy, are time consuming and can be inaccurate due to their 2D nature [12]; recent efforts [13] have resulted in the fast construction of maps of absolute CNT concentration via optical absorbance methods, validated by Raman spectroscopy.

Experimental studies clearly show a correlation between homogeneous CNT dispersion and high electrical conductivity [14], but only a few studies analysed this numerically. Tarlton et al. [15] studied the conductivity of CNT networks generated by three-dimensional (3D) random walks, including CNT agglomerates. Gong et al. [16] analysed two-phase models comprising regions of uniformly distributed CNTs containing spherical CNT agglomerates of equal size, simplifying the real material microstructure and requiring assumptions on several parameters, such as the size and CNT concentration of the two phases. Hu et al. used a resistor network [17, 18] to investigate the detrimental effect of the size of spherical CNT aggregate on the electrical conductivity.

This paper presents a modelling strategy allowing quantification of the effects of a non-uniform CNT dispersion. The multiscale predictions presented are informed exclusively by the probability density function of CNT concentration measured by Fisher and Shaffer [13] via

optical transmittance measurements, and contain a single length-scale parameter which quantifies the minimum size of the features observed in the microstructure. The simulations assume a good electrical contact of matrix and CNTs in regions of high CNT concentration. Monte Carlo FE analyses are performed at micron and mm scale: at micron scale we use a technique we recently developed [19], while the focus of this work is on the construction of a realistic RVE of non-uniform concentration at mm scale and on the corresponding numerical homogenisation. We compare the predictions to measurements and use the simulation strategy to explore the effects of different features of the microstructure upon the electrical conductivity of CNT-polymer composites.

2. Generating a realistic 3D representation of the microstructure

Most observations of the microstructure of CNT-polymer composites result in 2D images, such as those in Fisher and Shaffer [13]. Here we develop a procedure to obtain 3D representations of the material's microstructure starting from the probability density function of CNT concentration in such 2D measurements.

The map is discretized as a regular array of square cells of side s, taken here as the pixel size. Based on such discretization, the cumulative distribution F_{wt} of the CNT weight fraction is computed. The concentration maps in [13] display the structure of a random multi-phase composite, comprising an array of irregular regions of different size. For a statistically-isotropic microstructure, it is possible to define a feature size radius r_{f} (i.e. the radius of the regions of approximately uniform concentration found in the map) and the corresponding non-dimensional feature radius parameter $R_{\mathrm{f}} = r_{\mathrm{f}}/s$. We note that the map in Fisher and Shaffer [13] refers to a statistically isotropic material, as it was confirmed in preliminary experiments sectioning the material along three mutually perpendicular planes.

A cubic RVE is built as a regular array of N_{s}^3 cells of equal dimensions, N_{s} being the number of cells along each RVE edge. A random CNT concentration is attributed to each cell, consistent with the cumulative probability F_{wt}, using inverse transform sampling (Fig. 1a). The RVE has now features of size s; to enforce a certain feature size, the CNT concentration of each j-th cell ρ_j is filtered based on the value and distance to its near neighbours, as

$$\rho_j^* = \frac{\sum_{i \in N_j} w_j(\vec{x}_i)\rho_i}{\sum_{i \in N_j} w_j(\vec{x}_i)} \tag{1}$$

where N_j represents the neighbourhood of the j-th cell, within a radius R_f (expressed in non-dimensional terms, i.e. in number of cells), and $w_j(\vec{x})$ the weight function of a cell with centre at position $\vec{x}$ ($\vec{x}$ is normalised by the cell size s) with respect to the current cell j. The weight function is taken as a simple linearly decaying function

$$w_j(\vec{x}_i) = R_\mathrm{f} - \left\| \overrightarrow{x_i} - \vec{x}_j \right\| \tag{2}$$

where $\| \ \|$ denotes the 2-norm of its argument. This procedure is used in topology optimization [20] to enforce minimum feature sizes and avoid mesh size dependency. While a constant weight function would result in more distinct features, the linear decay results in a more continuous variation of concentration, similar to the observations we aim to reproduce. The filter is applied through the boundaries of the RVE in a periodic fashion (Fig. 1b and c). Since the density distribution is stored as a 3D array, which corresponds to a regular density distribution, the neighbouring cells can be simultaneously retrieved by rolling the array along all axes.

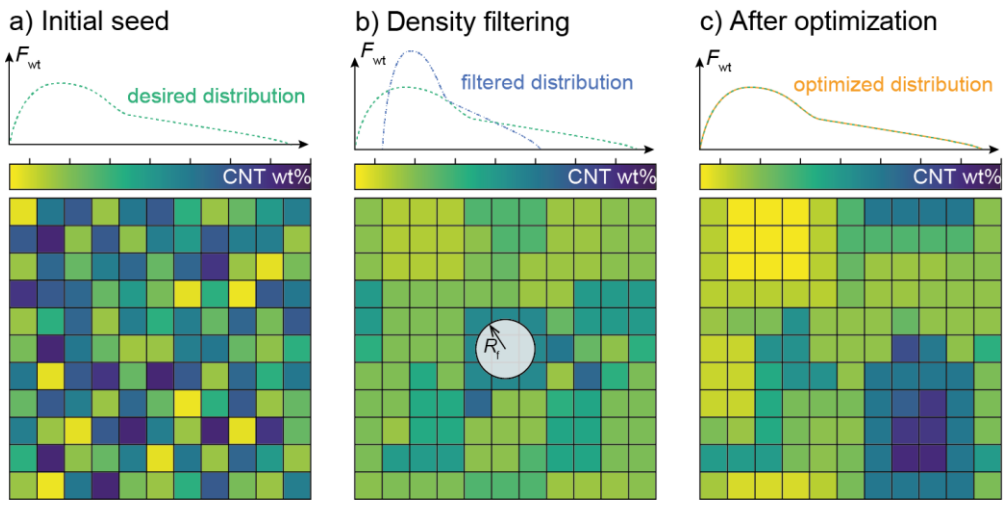

Fig. 1. Illustration of the proposed dispersion generation method: a) the initial random seed, b) changed upon filtering the CNT density and c) after the optimization procedure where both radius and distribution are respected.

This filtering procedure results in a narrower distribution of CNT concentrations; to correct this we proceed to modify the density distribution to respect both the feature radius R_f filter and the first four statistical moments m_k, here defined as: mean $m_1 = \mu_\rho$, standard deviation

$m_2 = \sigma_\rho$, skewness m_3 and kurtosis m_4. To achieve this, the density array is subjected to a gradient-based constrained optimization algorithm. A conservative, convex, separable approximation with quadratic separation [21] is used, as implemented in the NLopt library [22]. This optimization problem can be summarized as

$$\begin{aligned} \text{minimize:} \quad & f_0(\vec{\rho}) = \sum_{k=1}^{4} M_k\left(\vec{\rho}^*\right) \\ \text{subject to:} \quad & M_k(\vec{\rho}^*) - \delta_k \leq 0, \;\; k = 1, \dots, 4 \\ & \rho_{\min} \leq \rho_i \leq \rho_{\max}, \;\; i = 1, \dots, N_s^3 \end{aligned} \tag{3}$$

where $M_k = \left(m_k^{\text{real}} - m_k^{\text{spec}}\right)^2$ represents the squared distance between the real m_k^{real} and specified k-th moment m_k^{spec}, and δ_k a very small positive tolerance chosen (by trial and error) as 10^{-9}, to translate the constraint condition into an inequality, while allowing convergence within reasonable time. The minimum $\rho_{\min}$ and maximum $\rho_{\max}$ density are taken as the extrema of the initial observation. The design variables – i.e. the CNT density of each cell – are filtered at each iteration, together with the sensitivities (or derivatives) of the objective and constraint functions. The final iteration represents a 3D RVE (Fig. 1c) in which the CNT dispersion obeys the observed probability distributions and displays the required minimum feature size.

We note here that in the following numerical analysis we will construct 3D RVEs starting from a 2D dataset. However, the only quantitative information taken from the work of Fisher and Shaffer [13] is their measured probability density function of the CNT concentration, which can be reliably obtained from their 2D measurements.

3. Numerical modelling (FE)

The conductivity of the random RVEs is predicted by the finite element method (Abaqus Standard [23]) using steady-state heat transfer analyses, replacing all thermal properties with the appropriate electrical equivalents [24]. The cubic RVE is discretized into finite elements corresponding to the cells used in the discretisation. Different material sections are assigned to every element based on its CNT content. The corresponding conductivity is taken from the results of our micron-scale analysis of homogeneous RVEs, presented in detail in [19]; the properties of CNT and matrix, the length and aspect ratios of the CNTs and the properties of the tunnelling junctions between neighbouring CNTs will be provided below.

Electric periodic boundary conditions are enforced by constraining the electrical potential U degrees of freedom of nodes at opposing boundaries as

$$U^{l+} - U^{l-} = \bar{E}_l L_{\mathrm{RVE}} \tag{4}$$

where $(l+)$ and $(l-)$ correspond to the boundaries with positive and negative normal along the axis X_l, L_{RVE} is the distance between these two boundaries and $\bar{\mathbf{E}}$ is the homogenized electric field.

Three distinct load cases are created, enforcing a uniaxial homogenized electric field in the 3 Cartesian directions. By measuring, in each case, the current that flows through the volume in all 3 directions, the full homogenized conductivity matrix $\bar{\kappa}_{ij}$ is reconstructed.

4. Results and discussion

The proposed methodology is now compared to the measurements in [13], on CNT-polymer composites whose processing is described in [25].

The material consists of industrial grade multi-walled CNTs (NC7000, Nanocyl™) dispersed in an epoxy matrix [25]. To compute the conductivity of the composites, in the simulations we use CNT of length $L_{\mathrm{CNT}} = 430$ nm and diameter $D_{\mathrm{CNT}} = 10$ nm. A nanotube conductivity of 10^4 S/m [26] is assumed, with a work fraction of 4.95 eV. [27]. As for the epoxy matrix, a conductivity of 10^{-6} S/m and relative permittivity of 3.98 are chosen. Densities of 1.9 kg/m^3 and 1.2 kg/m^3 are used for the CNTs and matrix, respectively. We note that these parameters are not adjusted to maximise the agreement of the predictions with measurements: the density of the constituents as well as the diameter and average length of the CNTs were measured, while the CNT conductivity, work fraction and relative permittivity of the matrix (determining the tunnelling electron transport at CNT junctions) are taken from the literature. The sensitivity of the predictions to the values of these parameters was explored systematically (for the case of a uniform CNT concentration) in [28].

Considering a uniform and random dispersion, the homogenized isotropic conductivity curve is obtained using the FE approach presented in [19]. The results are obtained with 20 realizations per volume fraction and with a converged RVE size of $2.0 \times L_{\mathrm{CNT}}$; the predicted conductivity is presented in Fig. 2 together with the measurements of Herceg et al. [25]. We

direct the reader to [19] for further comments on the standard deviation of these predictions and how this varies with the CNT volume fraction.

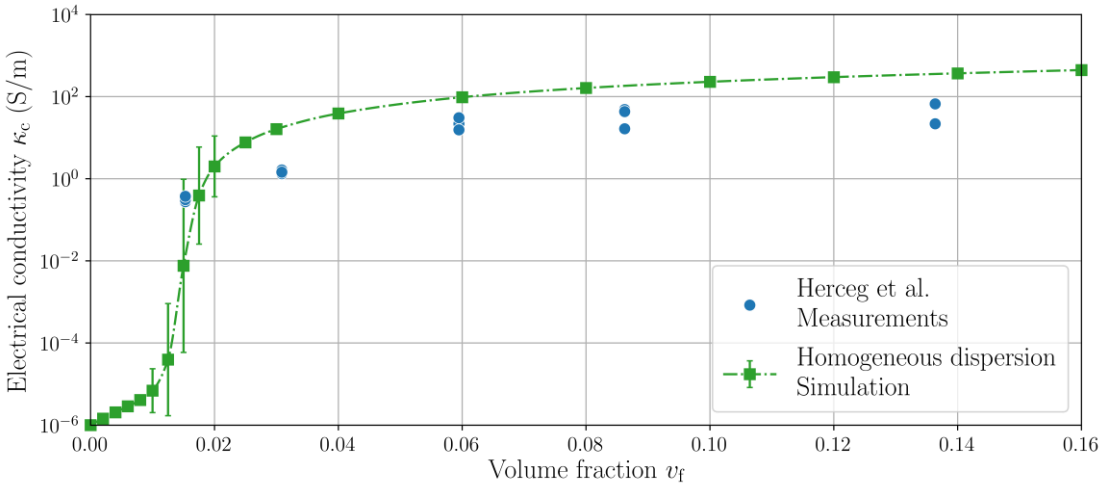

Fig. 2. Homogenized electrical conductivity as function of the CNT volume fraction. Bars represent the standard deviation and the experimental measurements are reproduced from Herceg et al. [**25**].

The assumption of homogeneous CNT dispersion clearly overestimates the measured conductivity above the percolation threshold – found around $v_{f_c} \simeq 1.5\%$ in the case of uniform CNT dispersion.

To quantify the effects of the dispersion, we rely on the CNT concentration map presented by Fisher and Shaffer [13] and reproduced in Fig. 3, based on a discretization of 100x100 cells.

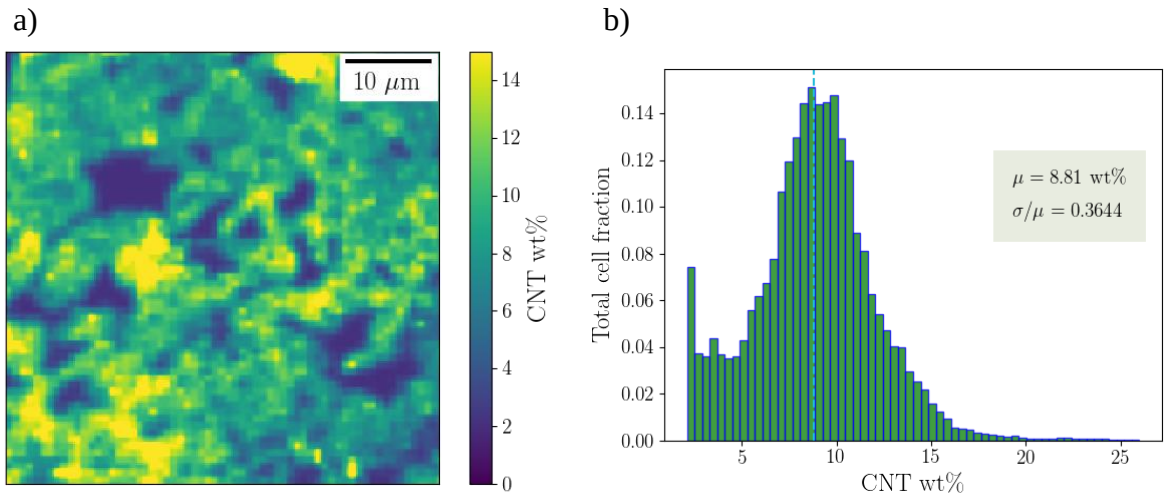

Fig. 3. a) Measured dispersion map image; b) concentration distribution, reproduced from [**13**].

According to [13], the sample was prepared with a CNT concentration of 9.1 wt%, based on initial weighing. In the concentration map in Fig. 3a however, the average measured concentration was 7.58 wt%. This discrepancy might be due to loss of CNTs (by decomposition) or to variability of the material microstructure over the length scale of observation, of approximately $1\ \mathrm{mm}^2$. The virtual RVEs constructed in this study are based on a slightly smaller section of the published image in Fig. 3a, to avoid editing artefacts (as softened intensity at the edges and the area covered by the legend), and corresponds to an average CNT concentration of 8.81 wt%, equivalent to a volume fraction of $v_\mathrm{f} = 5.75$ % (vol%). For the same concentration, Herceg et al. [25] measured a bulk conductivity in the range $15.5 - 22.0\ \mathrm{S/m}$.

We now construct different RVEs corresponding to the concentration distribution presented in Fig. 3b), using different feature radius parameters, to explore the sensitivity of our predictions to such length-scale. For each value of the feature radius we conduct an RVE convergence study, to ensure predictions are not sensitive to the size of the RVE analysed. For a feature radius of $R_\mathrm{f} = 5$, the resulting homogenized conductivity for 20 realizations is plotted in Fig. 4a) as function of the number of elements N_cell, resulting in meshes with 1000 to 1728000 elements. The average conductivity varies less than 1% for $N_\mathrm{cell} \geq 50^3$, and the standard deviation is less than 2% for $N_\mathrm{s} \geq 100^3$. A further indication that the RVE is of sufficiently large size can be obtained by measuring the cross-terms of the conductivity matrix $\bar{\kappa}_{ij}$ $(i \neq j)$, presented in Fig. 4b): a sufficiently large RVE will be statistically isotropic and will present vanishing cross-terms. Such RVE convergence analysis was repeated for all the feature radii investigated. It showed that RVEs with $N_\mathrm{cell} > 100^3$ provide predictions insensitive to size, and results shown in this section refer to the choice $N_\mathrm{cell} = 100^3$, corresponding to approximately 100 million elements and 103 million degrees of freedom.

It is worth noting that the observed convergence of the predictions with RVE size reinforces the notion of existence of a unique solution for a set of dispersion distribution and corresponding feature radius, an issue observed with some of the dispersion indexes, as discussed by Haslam and Raeymaekers [10].

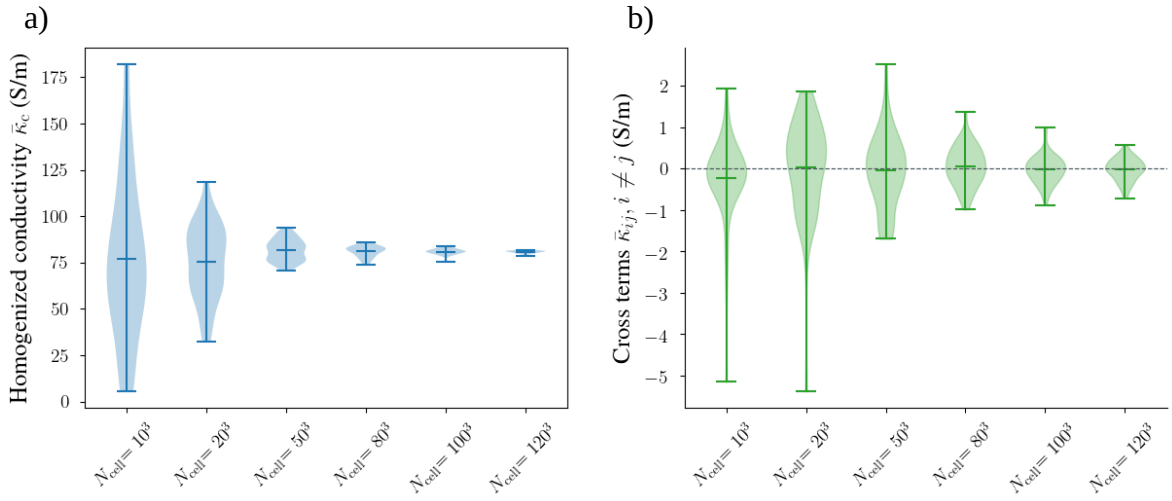

Fig. 4. RVE size convergence study, analysing the: a) homogenized conductivity and b) cross terms of the conductivity matrix.

We now perform a study of the effect of feature radius on the predictions of bulk conductivity. We construct a parametric model with only 1 parameter (the filter radius R_f), and build three-dimensional RVEs accordingly, satisfying the measured PDF of Fisher and Shaffer [13]. Then, the middle section (along the z coordinate) of RVEs with different filter radius are plotted in Fig. 5, to illustrate the morphology of the virtual microstructures investigated. From a qualitative visual comparison of the virtual microstructures in Fig. 5 to the measured microstructure in Fig. 3a it emerges that the real material microstructure is intermediate between the virtual microstructures obtained with filter radii 3.2, 5.0 and 8.0.

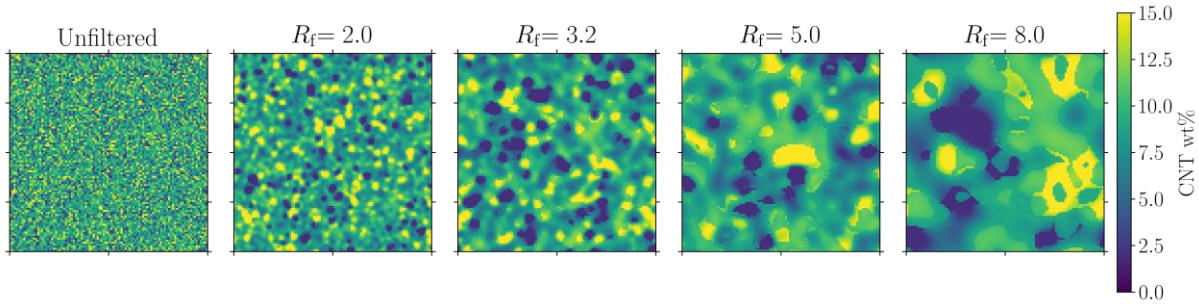

Fig. 5. **Central cross section (along the z direction) of RVEs with different feature radius.**

The predictions of homogenized electrical conductivity are plotted in **Error! Reference source not found.** for different values of feature radii (averages of 20 realizations are shown). We consider an unfiltered distribution when $R_f = 0.5$, representing a diameter equal to the cell length ($2r_f = s$). Clearly a non-uniform CNT concentration reduces the bulk conductivity, in a greater measure for large feature radii, although the predictions seem to plateau at approximately 80 S/m, with conductivity 11% less than for the case of a homogeneous concentration. We recall that measurements on this material gave conductivity in the range

$15.5 - 22.0\ \mathrm{S/m}$: our simulations suggest that such low values cannot be explained by the inhomogeneous concentration. In several published papers [5, 6, 29] a non-homogeneous CNT concentration is invoked to justify the discrepancy between the measured conductivity of these materials. Our simulations suggest that this is not entirely the case, and the reasons for such discrepancies must be sought elsewhere: for example, in the accuracy of both experimental techniques and nanoscale effects that influence the contact resistance between CNTs.

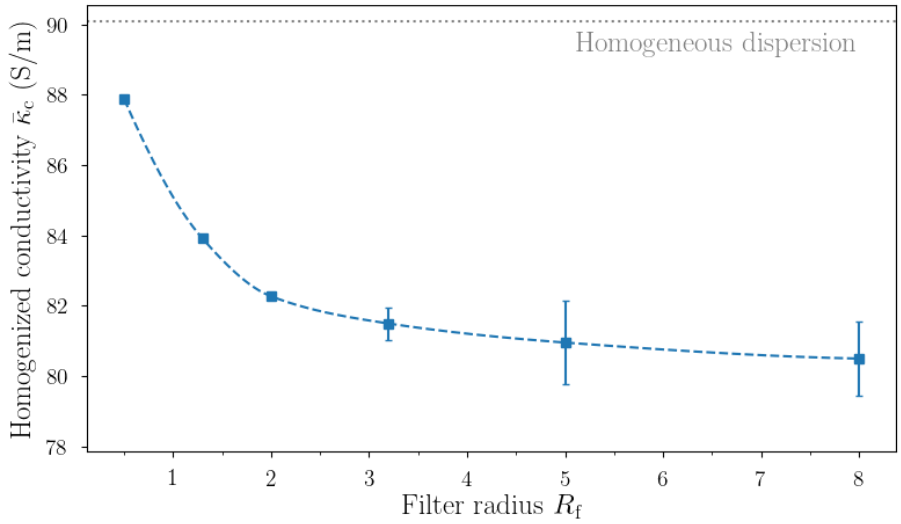

Fig. 6. Influence of the feature radius on the homogenized conductivity for the CNT-concentration distribution observed experimentally. Error bars represent standard deviation based on 20 realizations.

5. Sensitivity of the bulk conductivity to the details of CNT concentration

In this section we explore the sensitivity of conductivity predictions to the details of the CNT concentration, to show that such sensitivity is different at different points along the percolation curve. The CNT and epoxy properties presented in the previous section are used. The CNT concentration is assumed to follow a lognormal distribution, defined by an average v_f and the ratio of standard deviation to average volume fraction (relative standard deviation RSD, σ_ρ/μ_ρ). The lognormal distribution was chosen, in the parametric study, due to its flexibility and capability of modelling asymmetric probability density functions; the measured distributions of CNT concentration in real materials presented in the literature (e.g. [11, 13].) are in fact skewed towards small volume fractions. An illustration of the effect of σ_ρ/μ_ρ on the microstructure morphology is shown in Fig. 7 in the form of absorption maps. The concentrations were translated into absorption maps using the relationship presented by [13].

In the current section, RVEs are constructed for 3 different average CNT volume fractions, chosen to be clearly above percolation, approximately at percolation, and clearly below percolation. (Note: for CNT concentrations close and below percolation it was not always possible to construct a virtual microstructure, i.e. the optimizer was not able to find an RVE distribution that simultaneously respects the 4 statistical moments and the specified feature radius.. Hence, the corresponding results are not shown).

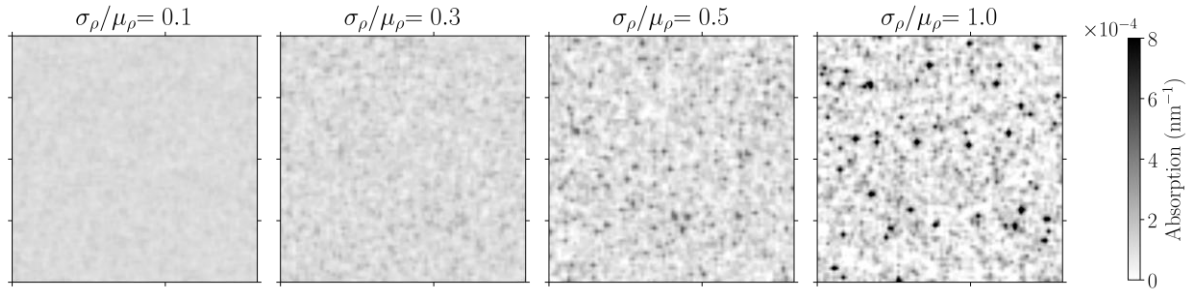

Fig. 7. Reconstructed absorption maps of CNT concentration for different RVEs with a CNT volume fraction of 2.6% and varying RSD, for a feature radius of $\boldsymbol{R}_\mathrm{f} = \mathbf{1.3}$.

- Above percolation ($v_\mathrm{f} = 6.0\ \%$). For a volume fraction of $v_\mathrm{f} = 6.0\ \%$, clearly above the percolation threshold for the CNT-polymer composite considered, in Fig. 8 we show the effects of RSD and feature radius on the bulk conductivity. Greater feature radius and RSD values reduce the predicted conductivity.
- Around percolation ($v_\mathrm{f} = 2.6\ \%$). At this CNT concentration, slightly above the percolation threshold, an anomalous behaviour is observed for the case of unfiltered concentration distribution $R_\mathrm{f} = 0.5$, as shown in Fig. 9. In this case the conductivity increases with increasing RSD, opposite to what is observed at larger feature radii (and in every case at higher volume fractions).
- Below percolation ($v_\mathrm{f} = 1.3\ \%$). Results for this volume fraction are shown in Fig. 10. Again, simulations suggest that conductivity can increase with increasing RSD. This observation is coherent with the findings published by [30], where experimental measurements revealed percolation bellow the expected threshold (this second threshold is usually referred to as a second kinetic, or non-statistical percolation threshold).

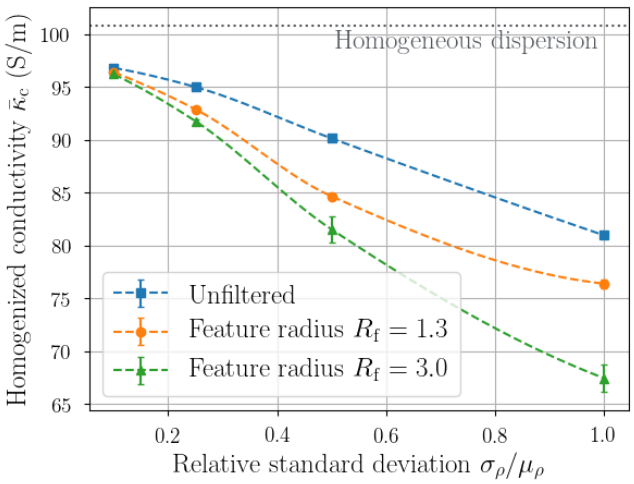

Fig. 8. Influence of the relative standard deviation and filter radius on conductivity, for a volume fraction of **6.0**%.

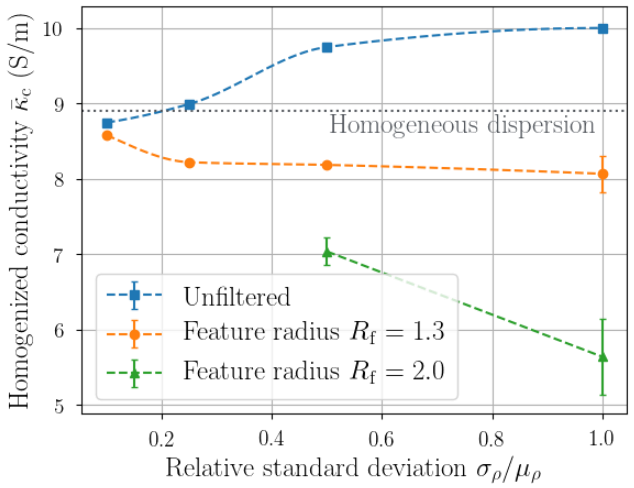

Fig. 9. Influence of the relative standard deviation and filter radius on the conductivity, for a volume fraction of **2.6**%.

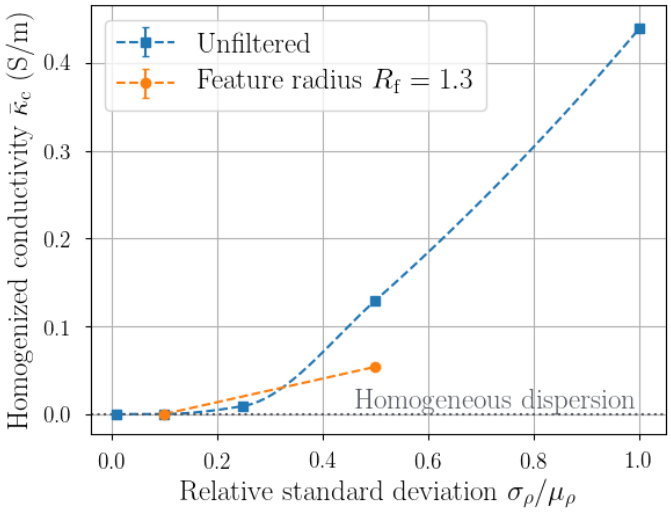

Fig. 10. Influence of the relative standard deviation and filter radius on the conductivity, for a volume fraction of 1.3%.

In Fig. 11 we summarise the results in this section: the inhomogeneity of CNT concentration has two obvious effects, often reported in the literature: (i) conductivity is enabled at lower volume fractions than in the uniform case, and (ii) at high CNT concentration, increasing inhomogeneity of CNT concentration reduces the conductivity. We note that with increasing CNT volume fraction the conductivity is less sensitive to the details of the heterogeneity in the distribution.

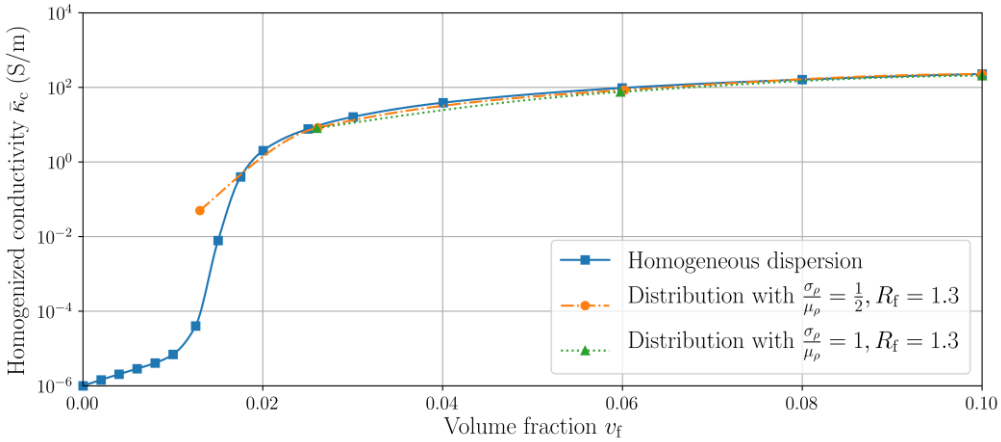

Fig. 11. Effect of dispersion on the percolation curve considering a lognormal distribution for the CNT concentration.

6. Conclusions

A multiscale approach to simulate the effects of a non-homogeneous CNT concentration in CNT-polymer composites was presented. We constructed realistic virtual microstructures of these composites based on measured probability density functions of CNT concentration, also including a single length-scale associated with the topology of the features observed in 2D concentration maps. We performed Monte Carlo analyses via the FE method to predict the bulk electrical conductivity of such realistic material microstructures at different values of the minimum feature size. The predictions were compared to measurements and used to determine the sensitivity of conductivity to the probability density of the CNT concentration and on the size of the geometric features observed in the microstructure. The main conclusions from the study are:

- The conductivity of heterogeneous CNT-polymer composites was found, in the range explored in the study, as much as 11% smaller than the conductivity of composites with uniform CNT concentration. This reduction is substantial but not sufficiently large to justify, on its own, the discrepancy between measurements and prediction often observed in previous studies.
- The size and distribution of the geometric features observed in realistic microstructures has a prominent effect in determining the conductivity of these composites. Such effect is comparable to that of the probability density function of CNT concentration. Increasing the size of these features decreases the conductivity irrespective of the average and distribution of the CNT volume fraction.
- An increasing degree of variance in the CNT volume fraction reduces the conductivity at high volume fractions but may increase it at volume fractions around the statistical percolation threshold and below, depending on the size of the geometric features observed in the microstructure.
- The effects of the variance in CNT volume fraction and of the feature size become less prominent with increasing average CNT concentration.

The work showed the importance of performing measurements similar to those in [13] in numerical predictions the electrical response of CNT-polymer composites. Such measurements could be also used to predict the self-sensing capability of realistic CNT-polymer composites, as shown in [31] for the case of a homogeneous CNT distribution. This is left as a topic for future studies.

7. Acknowledgments

This project was funded by the European Union's Horizon 2020 research and innovation program, under the Marie Skłodowska-Curie Grant Agreement no. 642890 (http://thelink-project.eu).

8. References

[1] W. Zhang, A.A. Dehghani-Sanij, R.S. Blackburn, Carbon based conductive polymer composites, J Mater Sci 42(10) (2007) 3408-3418.
[2] R. Strümpler, J. Glatz-Reichenbach, Feature Article: Conducting Polymer Composites, Journal of Electroceramics 3(4) (1999) 329-346.
[3] J.K.W. Sandler, J.E. Kirk, I.A. Kinloch, M.S.P. Shaffer, A.H. Windle, Ultra-low electrical percolation threshold in carbon-nanotube-epoxy composites, Polymer 44(19) (2003) 5893-5899.
[4] R.H. Baughman, A.A. Zakhidov, W.A. de Heer, Carbon nanotubes - the route toward applications, Science 297(5582) (2002) 787-792.
[5] W. Bauhofer, J.Z. Kovacs, A review and analysis of electrical percolation in carbon nanotube polymer composites, Compos Sci Technol 69(10) (2009) 1486-1498.
[6] P.-C. Ma, N.A. Siddiqui, G. Marom, J.-K. Kim, Dispersion and functionalization of carbon nanotubes for polymer-based nanocomposites: A review, Composites Part A: Applied Science and Manufacturing 41(10) (2010) 1345-1367.
[7] S. Bose, R.A. Khare, P. Moldenaers, Assessing the strengths and weaknesses of various types of pre-treatments of carbon nanotubes on the properties of polymer/carbon nanotubes composites: A critical review, Polymer 51(5) (2010) 975-993.
[8] Z.P. Luo, J.H. Koo, Quantifying the dispersion of mixture microstructures, Journal of Microscopy 225(2) (2007) 118-125.
[9] B.M. Tyson, R.K. Abu Al-Rub, A. Yazdanbakhsh, Z. Grasley, A quantitative method for analyzing the dispersion and agglomeration of nano-particles in composite materials, Composites Part B-Engineering 42(6) (2011) 1395-1403.
[10] M.D. Haslam, B. Raeymaekers, A composite index to quantify dispersion of carbon nanotubes in polymer-based composite materials, Composites Part B-Engineering 55 (2013) 16-21.
[11] S.R. Bakshi, R.G. Batista, A. Agarwal, Quantification of carbon nanotube distribution and property correlation in nanocomposites, Composites Part A: Applied Science and Manufacturing 40(8) (2009) 1311-1318.
[12] Y. Gao, Z. Li, Z.Y. Lin, L.J. Zhu, A. Tannenbaum, S. Bouix, C.P. Wong, Automated dispersion and orientation analysis for carbon nanotube reinforced polymer composites, Nanotechnology 23(43) (2012).
[13] S.J. Fisher, M.S.P. Shaffer, Rapid quantitative mapping of multi-walled carbon nanotube concentration in nanocomposites, Compos Sci Technol 160 (2018) 161-168.
[14] B. Krause, P. Pötschke, L. Häußler, Influence of small scale melt mixing conditions on electrical resistivity of carbon nanotube-polyamide composites, Compos Sci Technol 69(10) (2009) 1505-1515.
[15] T. Tarlton, E. Sullivan, J. Brown, P.A. Derosa, The role of agglomeration in the conductivity of carbon nanotube composites near percolation, Journal of Applied Physics 121(8) (2017) 9.

[16] S. Gong, Z.H. Zhu, J. Li, S.A. Meguid, Modeling and characterization of carbon nanotube agglomeration effect on electrical conductivity of carbon nanotube polymer composites, Journal of Applied Physics 116(19) (2014) 194306.
[17] N. Hu, Y. Karube, C. Yan, Z. Masuda, H. Fukunaga, Tunneling effect in a polymer/carbon nanotube nanocomposite strain sensor, Acta Mater 56(13) (2008) 2929-2936.
[18] N. Hu, Z. Masuda, C. Yan, G. Yamamoto, H. Fukunaga, T. Hashida, The electrical properties of polymer nanocomposites with carbon nanotube fillers, Nanotechnology 19(21) (2008) 215701.
[19] M.A.S. Matos, V.L. Tagarielli, P.M. Baiz-Villafranca, S.T. Pinho, Predictions of the electro-mechanical response of conductive CNT-polymer composites, J Mech Phys Solids 114 (2018) 84-96.
[20] M.P. Bendsoe, O. Sigmund, Topology Optimization: Theory, Methods, and Applications, Springer Berlin Heidelberg2013.
[21] K. Svanberg, A class of globally convergent optimization methods based on conservative convex separable approximations, Siam J Optimiz 12(2) (2002) 555-573.
[22] S.G. Johnson, The NLopt nonlinear-optimization package, (2014).
[23] D.S. Simulia, Abaqus 2018 Documentation, 2018.
[24] J.N. Reddy, An Introduction To The Finite Element Method, McGraw-Hill2006.
[25] T.M. Herceg, S.H. Yoon, M.S.Z. Abidin, E.S. Greenhalgh, A. Bismarck, M.S.P. Shaffer, Thermosetting nanocomposites with high carbon nanotube loadings processed by a scalable powder based method, Compos Sci Technol 127 (2016) 62-70.
[26] T.W. Ebbesen, H.J. Lezec, H. Hiura, J.W. Bennett, H.F. Ghaemi, T. Thio, Electrical conductivity of individual carbon nanotubes, Nature 382(6586) (1996) 54-56.
[27] M. Shiraishi, M. Ata, Work function of carbon nanotubes, Carbon 39(12) (2001) 1913-1917.
[28] M. A. S. Matos, S.T. Pinho and V.L. Tagarielli, (2019). Predictions of the electrical conductivity of composites of polymers and carbon nanotubes by an artificial neural network. Scripta Materialia, 166, 117–121.
[29] C.A. Martin, J.K.W. Sandler, M.S.P. Shaffer, M.K. Schwarz, W. Bauhofer, K. Schulte, A.H. Windle, Formation of percolating networks in multi-wall carbon-nanotube-epoxy composites, Compos Sci Technol 64(15) (2004) 2309-2316.
[30] J.Z. Kovacs, B.S. Velagala, K. Schulte, W. Bauhofer, Two percolation thresholds in carbon nanotube epoxy composites, Compos Sci Technol 67(5) (2007) 922-928.
[31] M. A. S. Matos, S.T. Pinho and V.L. Tagarielli (2019). Application of machine learning to predict the multiaxial strain-sensing response of CNT-polymer composites. Carbon, 146, 265–275.